

Saturation Effects in Hadronic Cross Sections*

ARIF I. SHOSHI AND FRANK D. STEFFEN

*Institut für Theoretische Physik, Universität Heidelberg
Philosophenweg 16 & 19, D-69120 Heidelberg, Germany*

Abstract

We compute total and differential elastic cross sections of high-energy hadronic collisions in the loop-loop correlation model that provides a unified description of hadron-hadron, photon-hadron, and photon-photon reactions. The impact parameter profiles of pp and γ^*p collisions are calculated. For ultra-high energies the hadron opacity saturates at the black disc limit which tames the growth of the hadronic cross sections in agreement with the Froissart bound. We compute the impact parameter dependent gluon distribution of the proton $xG(x, Q^2, |\mathbf{b}_\perp|)$ and find gluon saturation at small Bjorken x . These saturation effects manifest S-matrix unitarity in hadronic collisions and should be observable in future cosmic ray and accelerator experiments at ultra-high energies. The c.m. energies and Bjorken x at which saturation sets in are determined and LHC and THERA predictions are given.

*Talk presented by F. D. Steffen at the 14th Topical Conference on Hadron Collider Physics, Karlsruhe, Germany, September 29 – October 4, 2002

Saturation Effects in Hadronic Cross Sections

Arif I. Shoshi and Frank D. Steffen

Institut für Theoretische Physik, Universität Heidelberg
Philosophenweg 16 & 19, D-69120 Heidelberg, Germany

1 Introduction

The steep rise of the gluon distribution $xG(x, Q^2)$ and structure function $F_2(x, Q^2)$ of the proton towards small Bjorken $x = Q^2/s$ is one of the most exciting observations at the HERA experiments [1]. The experimental results show a rise of the total γ^*p cross section, $\sigma_{\gamma^*p}^{tot}(s, Q^2)$, with increasing c.m. energy \sqrt{s} which becomes stronger with increasing photon virtuality Q^2 . In hadronic interactions, the rise of the total cross sections is limited: The Froissart bound, derived from very general principles such as unitarity and analyticity of the S -matrix, allows at most a logarithmic energy dependence of the cross sections at asymptotic energies [2]. Analogously, the rise of $\sigma_{\gamma^*p}^{tot}(s, Q^2)$ is expected to slow down. The microscopic picture behind this slow-down is the concept of gluon saturation: Since the gluon density in the proton becomes large at high energies \sqrt{s} (small x), gluon fusion processes are expected to tame the growth of $\sigma_{\gamma^*p}^{tot}(s, Q^2)$, and it is a key issue to determine the energy at which these processes become significant.

In this talk we give predictions for saturation effects in hadronic cross sections using the loop-loop correlation model (LLCM) that provides a unified description of hadron-hadron, photon-hadron, and photon-photon reactions [3]. The saturation effects are in agreement with S -matrix unitarity constraints and result from multiple gluonic interactions between the scattered particles. We show how these manifestations of S -matrix unitarity can in principle be observed in future cosmic ray and accelerator experiments at ultra-high energies. The c.m. energies and Bjorken x at which saturation sets in are determined and LHC and THERA predictions are given. The presented results are extracted from [3] where more details can be found.

2 The Loop-Loop Correlation Model

The loop-loop correlation model (LLCM) [3] is based on the functional integral approach to high-energy collisions [4–7]. Accordingly, the T -matrix element for elastic proton-proton (pp) scattering at c.m. energy squared s

and transverse momentum transfer \mathbf{q}_\perp ($t = -\mathbf{q}_\perp^2$) reads

$$T_{pp}(s, t) = 2is \int d^2b_\perp e^{i\mathbf{q}_\perp \cdot \mathbf{b}_\perp} J_{pp}(s, |\mathbf{b}_\perp|) \quad (1)$$

$$J_{pp}(s, |\mathbf{b}_\perp|) = \int dz_1 d^2r_1 \int dz_2 d^2r_2 |\psi_p(z_1, \mathbf{r}_1)|^2 |\psi_p(z_2, \mathbf{r}_2)|^2 \times [1 - S_{DD}(s, \mathbf{b}_\perp, z_1, \mathbf{r}_1, z_2, \mathbf{r}_2)] \quad (2)$$

where the correlation of two light-like Wegner-Wilson loops

$$S_{DD}(s, \mathbf{b}_\perp, \dots) = \left\langle W[C_1]W[C_2] \right\rangle_G \text{ with } W[C_i] = \frac{1}{3} \text{Tr } \mathcal{P} \exp \left[-ig \oint_{C_i} dz^\mu \mathcal{G}_\mu(z) \right] \quad (3)$$

describes the elastic scattering of two light-like color dipoles (DD) with transverse size and orientation \mathbf{r}_i and longitudinal quark momentum fraction z_i at impact parameter \mathbf{b}_\perp , i.e. the loops C_i represent the trajectories of the scattering color dipoles. For elastic pp scattering, the color dipoles are given in a simplified picture by a quark and diquark in each proton with \mathbf{r}_i and z_i distributions described by the simple phenomenological Gaussian wave function $|\psi_p(z_i, \mathbf{r}_i)|^2$. For reactions involving (virtual) photons, the quark and antiquark in the photon form a color dipole whose \mathbf{r}_i and z_i distribution is described by the perturbatively derived photon wave function $|\psi_{\gamma_{T,L}^*}(z_i, \mathbf{r}_i, Q^2)|^2$. To account for the non-perturbative region of low Q^2 in the photon wave function, quark masses $m_f(Q^2)$ are used that interpolate between current quarks at large Q^2 and constituent quarks at small Q^2 [8].

In contrast to the wave functions, the loop-loop correlation function S_{DD} is universal for pp , γ^*p , and $\gamma\gamma$ reactions [3]. We compute S_{DD} in the Berger-Nachtmann approach [9], in which S -matrix unitarity is respected, and describe the QCD interactions between the color dipoles by combining the non-perturbative stochastic vacuum model [10] with perturbative gluon exchange. This combination allows us to describe long and short distance correlations in agreement with numerical lattice computations [11] and leads to the static quark-antiquark potential with color Coulomb behavior for small source separations and confining linear rise for large source separations [12]. Two components are obtained of which the perturbative (P) component, $(\chi^P)^2$, describes two-gluon exchange and the non-perturbative (NP) component, $(\chi^{NP})^2$, the corresponding non-perturbative two-point interaction [13]. Ascribing a weak ($\epsilon^{NP} = 0.125$) and strong ($\epsilon^P = 0.73$) powerlike energy dependence to the non-perturbative and perturbative component, respectively,

$$\chi^{NP}(s)^2 = (\chi^{NP})^2 \left(\frac{s}{s_0} \frac{\mathbf{r}_1^2 \mathbf{r}_2^2}{R_0^4} \right)^{\epsilon^{NP}} \quad \text{and} \quad \chi^P(s)^2 = (\chi^P)^2 \left(\frac{s}{s_0} \frac{\mathbf{r}_1^2 \mathbf{r}_2^2}{R_0^4} \right)^{\epsilon^P}, \quad (4)$$

our final result for S_{DD} reads

$$S_{DD} = \frac{2}{3} \cos \left[\frac{1}{3} \chi^{NP}(s) \right] \cos \left[\frac{1}{3} \chi^P(s) \right] + \frac{1}{3} \cos \left[\frac{2}{3} \chi^{NP}(s) \right] \cos \left[\frac{2}{3} \chi^P(s) \right]. \quad (5)$$

The cosine functions ensure the unitarity condition in impact parameter space as they average to zero in the integration over the dipole orientations at very high energies. In fact, the higher order terms in the expansion of the cosine functions describe multiple gluonic interactions that are crucial for the saturation effects shown below: They tame the rise of hadronic cross sections and the gluon distribution in the proton $xG(x, Q^2)$ at ultra-high energies [3].

3 Saturation in Proton-Proton Scattering

The profile function (2) is a measure for the blackness or opacity of the interacting protons and gives an intuitive geometrical picture for the energy dependence of pp reactions: As shown in Fig. 1, the protons become blacker and larger with increasing c.m. energy \sqrt{s} . At ultra-high energies, $\sqrt{s} \gtrsim 10^6$ GeV, the opacity saturates at the black disc limit first for zero impact parameter while the transverse expansion of the protons continues. For purely imaginary elastic amplitudes, expected at high energies, the black disc limit is a strict unitarity bound that limits the height of the profile function at $J_{pp}^{\max} = 1$ for proton wave functions normalized to one. Thus, the saturation of the profile function is an explicit manifestation of S -matrix unitarity.

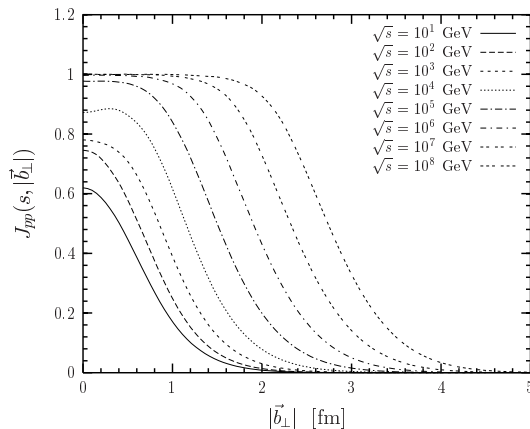


Fig. 1. The profile function for proton-proton scattering $J_{pp}(s, |\mathbf{b}_\perp|)$ as a function of the impact parameter $|\mathbf{b}_\perp|$ for c.m. energies from $\sqrt{s} = 10$ GeV to 10^8 GeV

The total pp cross section is obtained directly from the profile function (2)

$$\sigma_{pp}^{tot}(s) = \frac{1}{s} \text{Im} T_{pp}(s, t=0) = 2 \int d^2 b_\perp J_{pp}(s, |\mathbf{b}_\perp|) . \quad (6)$$

and shows saturation effects in principle observable in experiments. As can be seen in Fig. 2, the saturation of $J_{pp}(s, |\mathbf{b}_\perp|)$ tames the growth of $\sigma_{pp}^{tot}(s)$: There

is a transition from a power-like to an \ln^2 -increase of $\sigma_{pp}^{tot}(s)$, which respects the Froissart bound [2], at about $\sqrt{s} \approx 10^3$ TeV. Thus – according to our model – the onset of the black disc limit in pp collisions is about two orders of magnitude beyond LHC energy $\sqrt{s} = 14$ TeV and clearly out of reach for accelerator experiments in the near future. Here cosmic ray experiments might help that have access to energies of up to about 10^8 TeV.

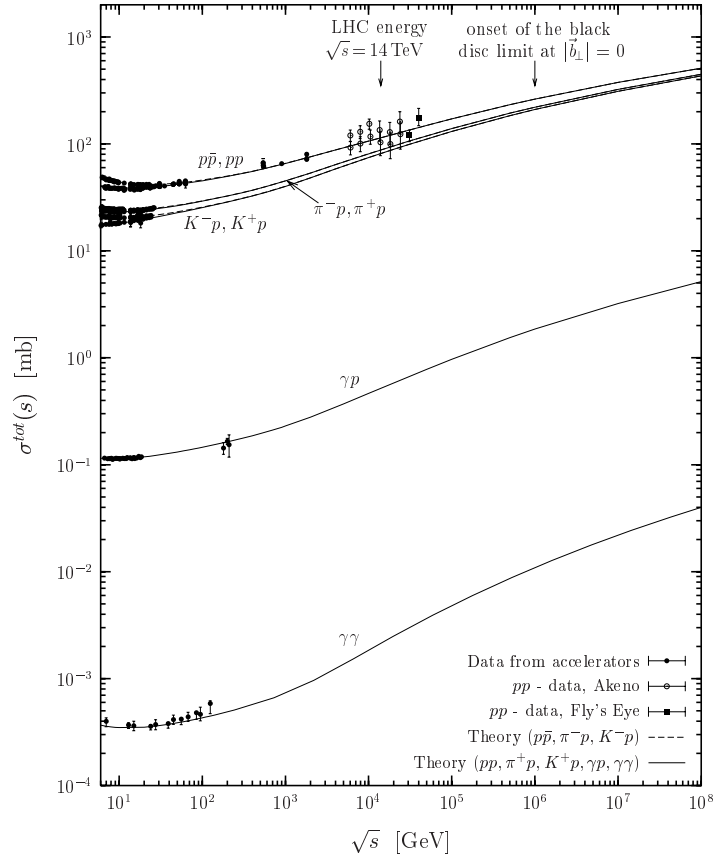


Fig. 2. The total cross section σ^{tot} as a function of the c.m. energy \sqrt{s} for pp , $p\bar{p}$, $\pi^\pm p$, $K^\pm p$, γp and $\gamma\gamma$ scattering. The solid lines represent the LLCM results for pp , $\pi^\pm p$, $K^\pm p$, γp and $\gamma\gamma$ scattering and the dashed lines the ones for $p\bar{p}$, $\pi^- p$, and $K^- p$ scattering. The pp , $p\bar{p}$, $\pi^\pm p$, $K^\pm p$, γp [14] and $\gamma\gamma$ data [15] taken at accelerators are indicated by the closed circles while the closed squares (Fly’s eye data) [16] and the open circles (Akeno data) [17] indicate cosmic ray data

The evolution of the profile function towards its saturation at the black disc limit is already interesting below $\sqrt{s} \approx 10^3$ TeV. Here the key quantity

is the differential elastic cross section which is obtained for purely imaginary T -matrix elements by Fourier transforming the profile function (2)

$$\frac{d\sigma_{pp}^{el}}{dt}(s, t) = \frac{1}{16\pi s^2} |T_{pp}(s, t)|^2 = \frac{1}{4\pi} \left[\int d^2 b_{\perp} e^{i\mathbf{q}_{\perp} \cdot \mathbf{b}_{\perp}} J_{pp}(s, |\mathbf{b}_{\perp}|) \right]^2. \quad (7)$$

Thus, the agreement of our model results with the data up to $\sqrt{s} = 1.8$ TeV shown in Fig. 3 is an important verification of the profiles shown in Fig. 1 up to $\sqrt{s} = 10^3$ GeV. The deviations from the data in the dip region are not

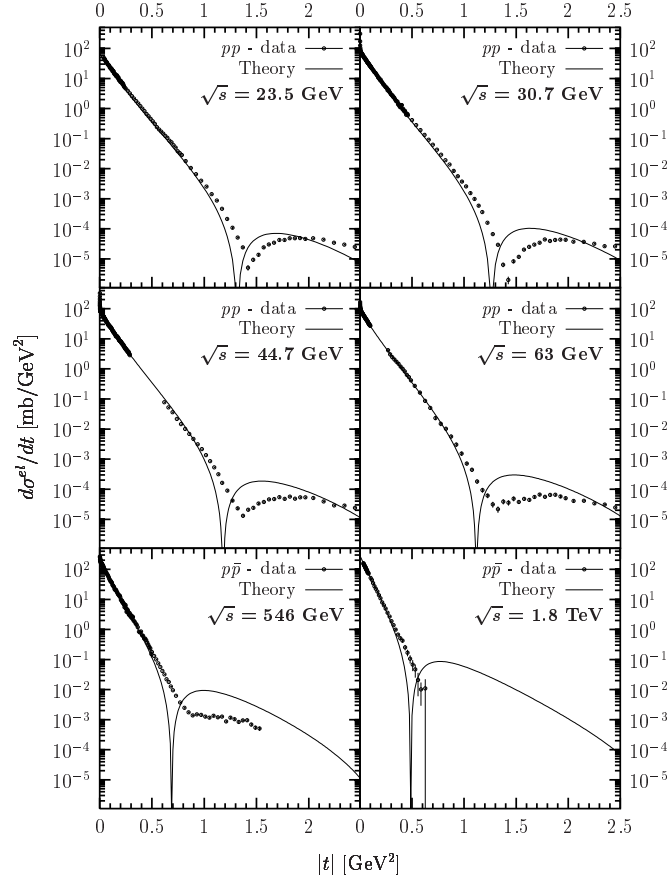


Fig. 3. The differential elastic cross section for pp and $p\bar{p}$ scattering as a function of the squared momentum transfer $|t|$. The LLCM results (*solid line*) are compared for $\sqrt{s} = 23.5, 30.7, 44.7$ and 63 GeV to the CERN ISR pp data [18], for $\sqrt{s} = 546$ GeV to the CERN $SppS$ data [19], and for $\sqrt{s} = 1.8$ TeV to Fermilab Tevatron $p\bar{p}$ data [20, 21] (*open circles*)

surprising since we work with a purely imaginary T -matrix element [3]. A real part is expected to be important in the dip region which is negligible in comparison to the imaginary part in the small $|t|$ region. Moreover, our model describes the pomeron ($C = +1$) contribution but not the odderon ($C = -1$) contribution important for the difference between pp and $p\bar{p}$ reactions.

It will be very interesting to see the pp differential elastic cross section measured at LHC and the associated profile function. Our prediction for $d\sigma_{pp}^{el}/dt$ at $\sqrt{s} = 14$ TeV is shown in Fig. 4. The associated profile is close to the dotted line in Fig. 1 and thus below the black disc limit.

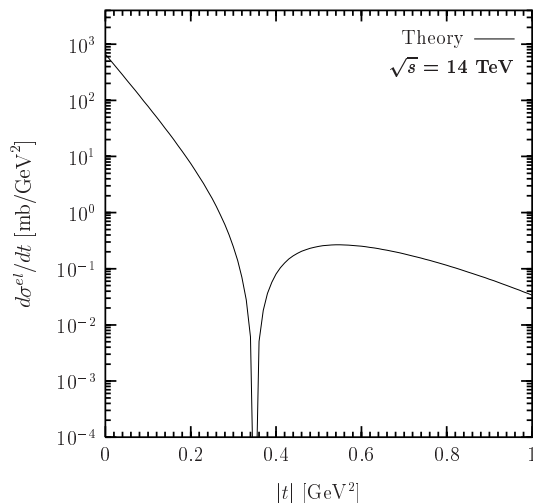


Fig. 4. The LLCM prediction of the pp differential elastic cross section at LHC ($\sqrt{s} = 14$ TeV) as a function of the squared momentum transfer $|t|$

4 Gluon Saturation

Based on the close relationship between the longitudinal structure function $F_L(x, Q^2)$ and the gluon distribution of the proton $xG(x, Q^2)$ at small x , the impact parameter dependent gluon distribution $xG(x, Q^2, |\mathbf{b}_\perp|)$ has been related to the profile function [3] $J_{\gamma_L^* p}(s = Q^2/x, |\mathbf{b}_\perp|, Q^2)$

$$xG(x, Q^2, |\mathbf{b}_\perp|) \approx 1.305 \frac{Q^2}{\pi^2 \alpha_s} \frac{\pi}{\alpha} J_{\gamma_L^* p}(0.417x, |\mathbf{b}_\perp|, Q^2). \quad (8)$$

Consequently, the shape of $xG(x, Q^2, |\mathbf{b}_\perp|)$ is determined by the profile function $J_{\gamma_L^* p}(s, |\mathbf{b}_\perp|, Q^2)$ which is obtained from (2) by replacing $|\psi_p(z_1, \mathbf{r}_1)|^2$

with the squared light-cone wave function for a longitudinally polarized photon $|\psi_{\gamma_L^*}(z_1, \mathbf{r}_1, Q^2)|^2$ [22]. Thus, the blackness described by the profile function is a measure for the gluon distribution and the black disc limit corresponds to the maximum of the gluon distribution that can be reached at a given impact parameter. In accordance with the behavior of the profile function $J_{\gamma_L^* p}$, see Fig. 5a, the gluon distribution $xG(x, Q^2, |\mathbf{b}_\perp|)$ decreases with increasing impact parameter for given values of x and Q^2 . The gluon density, consequently, has its maximum in the geometrical center of the proton, i.e. at zero impact parameter, and decreases towards the periphery. With decreasing x at given Q^2 , the gluon distribution $xG(x, Q^2, |\mathbf{b}_\perp|)$ increases and extends towards larger impact parameters just as the profile function $J_{\gamma_L^* p}$ for increasing s . The saturation of the gluon distribution $xG(x, Q^2, |\mathbf{b}_\perp|)$ sets in first in the center of the proton, $|\mathbf{b}_\perp| = 0$, at very small Bjorken x .

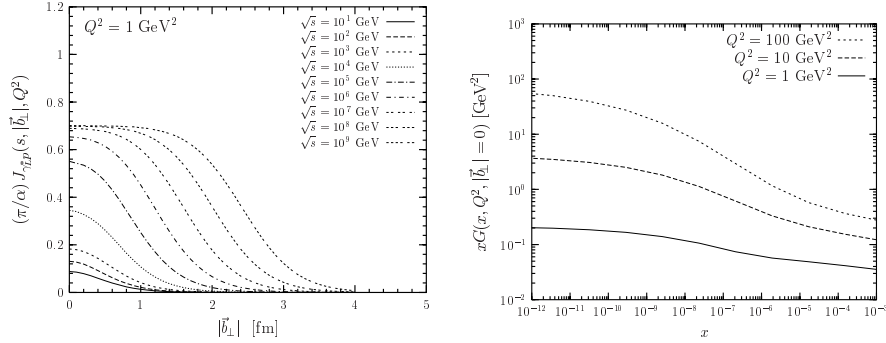


Fig. 5. (a) The profile function $(\pi/\alpha)J_{\gamma_L^* p}(s, |\mathbf{b}_\perp|, Q^2)$ as a function of the impact parameter $|\mathbf{b}_\perp|$ at photon virtuality $Q^2 = 1 \text{ GeV}^2$ for c.m. energies from $\sqrt{s} = 10 \text{ GeV}$ to 10^9 GeV . (b) The gluon distribution of the proton at zero impact parameter, $xG(x, Q^2, |\mathbf{b}_\perp| = 0)$, as a function of $x = Q^2/s$ for $Q^2 = 1, 10$ and 100 GeV^2

Using a proton wave function normalized to one, the black disc limit is given by the normalization of the longitudinal photon wave function

$$J_{\gamma_L^* p}^{max}(Q^2) = \int dz d^2 r |\psi_{\gamma_L^*}(z, \mathbf{r}, Q^2)|^2, \quad (9)$$

which depends on the photon virtuality Q^2 . This limit $J_{\gamma_L^* p}^{max}(Q^2)$ induces the upper bound on $xG(x, Q^2, |\mathbf{b}_\perp|)$ and determines the low- x saturation value

$$xG(x, Q^2, |\mathbf{b}_\perp|) \leq xG^{max}(Q^2) \approx 1.305 \frac{Q^2}{\pi^2 \alpha_s} \frac{\pi}{\alpha} J_{\gamma_L^* p}^{max}(Q^2) \approx \frac{Q^2}{\pi^2 \alpha_s}, \quad (10)$$

which is consistent with complementary investigations [23] and indicates strong color field strengths $G_{\mu\nu}^a \sim 1/\sqrt{\alpha_s}$ as well.

In Fig. 5b, the small- x saturation of the gluon distribution at zero impact parameter $xG(x, Q^2, |\mathbf{b}_\perp| = 0)$ is illustrated for $Q^2 = 1, 10$ and 100 GeV^2 as obtained in the LLCM. The saturation occurs at very low values of $x \lesssim 10^{-10}$ for $Q^2 \gtrsim 1 \text{ GeV}^2$. The photon virtuality Q^2 determines the saturation value (10) and the Bjorken x at which it is reached: For larger Q^2 , the small- x saturation value is larger and is reached at smaller values of x . Moreover, the growth of $xG(x, Q^2, |\mathbf{b}_\perp| = 0)$ with decreasing x becomes stronger with increasing Q^2 . This results from the stronger energy increase of the perturbative component in the LLCM, $\epsilon^P = 0.73$, that becomes more important with decreasing dipole size. In conclusion, our approach predicts the onset of the $xG(x, Q^2, |\mathbf{b}_\perp|)$ saturation for $Q^2 \gtrsim 1 \text{ GeV}^2$ at $x \lesssim 10^{-10}$ which is far below the x -region accessible at HERA ($x \gtrsim 10^{-6}$) and THERA ($x \gtrsim 10^{-7}$).

Note that the S -matrix unitarity condition together with relation (8) requires the saturation of the impact parameter dependent gluon distribution $xG(x, Q^2, |\mathbf{b}_\perp|)$ but not the saturation of the integrated gluon distribution $xG(x, Q^2)$. Indeed, approximating $xG(x, Q^2, |\mathbf{b}_\perp|)$ in the saturation regime by a step-function, $xG(x, Q^2, |\mathbf{b}_\perp|) \approx xG^{max}(Q^2) \Theta(R(x, Q^2) - |\mathbf{b}_\perp|)$, where $R(x, Q^2)$ denotes the full width at half maximum of the profile function, one obtains

$$xG(x, Q^2) \approx 1.305 \frac{Q^2 R^2(x, Q^2)}{\pi \alpha_s} \frac{\pi}{\alpha} J_{\gamma_L^* p}^{max}(Q^2) \approx \frac{Q^2 R^2(x, Q^2)}{\pi \alpha_s}, \quad (11)$$

which does not saturate because of the increase of the effective proton radius $R(x, Q^2)$ with decreasing x . Nevertheless, although $xG(x, Q^2)$ does not saturate, the saturation of $xG(x, Q^2, |\mathbf{b}_\perp|)$ leads to a slow-down in its growth towards small x .

5 Conclusion

We have computed saturation effects in hadronic cross sections with the loop-loop correlation model (LLCM). The LLCM combines perturbative and non-perturbative QCD in agreement with lattice investigations, provides a unified description of pp , γ^*p , and $\gamma\gamma$ reactions, and respects the S -matrix unitarity condition in impact parameter space. We have calculated impact parameter profiles of pp collisions in good agreement with the data for total and differential elastic cross sections. Predictions for measurements of these cross sections at the LHC were given. While the effective transverse expansion of the proton continues with increasing c.m. energy, the proton opacity in pp collisions saturates at the black disc limit for ultra-high energies of $\sqrt{s} \gtrsim 10^6 \text{ GeV}$ according to our model. This saturation tames the growth of the total pp cross section in agreement with the Froissart bound. We have computed the impact parameter dependent gluon distribution of the proton $xG(x, Q^2, |\mathbf{b}_\perp|)$ from the profile function for γ_L^*p reactions. The corresponding black disc limit is given by the normalization of the photon wave function and imposes a unitarity bound on $xG(x, Q^2, |\mathbf{b}_\perp|)$. Accordingly, the impact parameter dependent

gluon distribution $xG(x, Q^2, |\mathbf{b}_\perp|)$ saturates for $Q^2 \gtrsim 1 \text{ GeV}^2$ at $x \lesssim 10^{-10}$, which tames the steep rise of the integrated gluon distribution $xG(x, Q^2)$ towards small x .

References

1. C. Adloff *et al.* [H1 Collaboration]: Nucl. Phys. B **497**, 3 (1997); Eur. Phys. J. C **19**, 269 (2001); Eur. Phys. J. C **21**, 33 (2001);
J. Breitweg *et al.* [ZEUS Collaboration]: Phys. Lett. B **407**, 432 (1997); Phys. Lett. B **487**, 53 (2000).
2. M. Froissart: Phys. Rev. **123**, 1053 (1961).
3. A. I. Shoshi, F. D. Steffen and H. J. Pirner: Nucl. Phys. A **709**, 131 (2002).
4. O. Nachtmann: Annals Phys. **209**, 436 (1991).
5. H. G. Dosch, E. Ferreira and A. Krämer: Phys. Rev. D **50**, 1992 (1994).
6. O. Nachtmann: ‘High Energy Collisions And Nonperturbative QCD’. In: *Perturbative and Nonperturbative Aspects of Quantum Field Theory*, ed. by H. Latal and W. Schweiger (Springer, Berlin, Heidelberg 1997).
7. H. G. Dosch: ‘Nonperturbative Methods in QCD’. In: *Hadron Physics 96*, ed. by E. Ferreira *et al.*, (World Scientific, Singapore 1997).
8. H. G. Dosch, T. Gousset and H. J. Pirner: Phys. Rev. D **57**, 1666 (1998).
9. E. R. Berger and O. Nachtmann: Eur. Phys. J. C **7**, 459 (1999).
10. H. G. Dosch: Phys. Lett. B **190**, 177 (1987);
H. G. Dosch and Y. A. Simonov: Phys. Lett. B **205**, 339 (1988).
11. G. S. Bali, N. Brambilla and A. Vairo: Phys. Lett. B **421**, 265 (1998);
E. Meggiolaro: Phys. Lett. B **451**, 414 (1999).
12. A. I. Shoshi, F. D. Steffen, H. G. Dosch and H. J. Pirner: ‘Confining QCD Strings, Casimir Scaling, and a Euclidean Approach to High-Energy Scattering’, hep-ph/0211287.
13. A. I. Shoshi, F. D. Steffen, H. G. Dosch and H. J. Pirner: ‘Decomposition of the QCD String into Dipoles and Unintegrated Gluon Distributions’, hep-ph/0207287; Phys. Rev. **D** in press.
14. D. E. Groom *et al.* [Particle Data Group]: Eur. Phys. J. C **15**, 1 (2000).
15. G. Abbiendi *et al.* [OPAL Collaboration]: Eur. Phys. J. C **14**, 199 (2000);
M. Acciarri *et al.* [L3 Collaboration]: Phys. Lett. B **519**, 33 (2001).
16. R. M. Baltrusaitis *et al.*: Phys. Rev. Lett. **52**, 1380 (1984);
T. K. Gaisser, U. Sukhatme and G. B. Yodh: Phys. Rev. D **36**, 1350 (1987).
17. M. Honda *et al.*: Phys. Rev. Lett. **70**, 525 (1993);
N. N. Nikolaev, Phys. Rev. D **48**, 1904 (1993).
18. U. Amaldi and K. R. Schubert: Nucl. Phys. B **166**, 301 (1980).
19. M. Bozzo *et al.* [UA4 Collaboration]: Phys. Lett. B **147**, 385 (1984).
20. N. A. Amos *et al.* [E710 Collaboration]: Phys. Rev. Lett. **63**, 2784 (1989).
21. N. A. Amos *et al.* [E-710 Collaboration]: Phys. Lett. B **243**, 158 (1990).
22. A. I. Shoshi, F. D. Steffen and H. J. Pirner: ‘Gluon Saturation and S-matrix Unitarity’, hep-ph/0205343.
23. A. H. Mueller and J. Qiu: Nucl. Phys. B **268**, 427 (1986);
A. H. Mueller: Nucl. Phys. B **558**, 285 (1999);
E. Iancu and L. D. McLerran: Phys. Lett. B **510**, 145 (2001).